



Assessment of a solar-driven cogeneration system for electricity and desalination

Alireza Rafiei¹ · Reyhaneh Loni² · Gholamhassan Najafi² · Shuhaimi B. Mahadzir¹ · Evangelos Bellos³ · Mohsen Sharifpur^{4,5} · Mohamed Mazlan⁶

Received: 11 June 2020 / Accepted: 22 December 2020 / Published online: 5 February 2021
© Akadémiai Kiadó, Budapest, Hungary 2021

Abstract

The goal of the present paper is the investigation of a solar desalination system with an organic Rankine cycle system for power and freshwater production. This system is an environmentally friendly technology that is able to utilize solar energy properly in a novel cogeneration application. A parabolic trough concentrator with a smooth and corrugated receiver was employed as the heat source of the desalination system. A humidifier–dehumidifier desalination technology was used for producing freshwater. The electricity is produced by an organic Rankine cycle which is fed both by the solar field and by the hot brine. The present analysis is performed by using a detailed numerical model which is validated by experimental literature data. Based on the final results, the corrugated tube has a maximum performance of 66.59%, and it is more efficient than the smooth tube with 63.11%. The average freshwater productions were estimated equal to 13.09 kg hr⁻¹ and 12.71 kg hr⁻¹ for the corrugated and smooth tubes, respectively. The maximum net work production is found at 7.57 kW with R113, while the less efficient working fluid is R134a. It was found that the application of the developed desalination system leads to the production of high amounts of fresh water and a significant reduction of the equivalent CO₂ emissions.

Keywords Parabolic trough collector · Organic Rankine cycle · Cogeneration · Solar desalination · Environmental analysis

List of symbols

Solar modeling

A Area, m²
 c_2 Constant used in the linear equation

✉ Mohsen Sharifpur
mohsen.sharifpur@up.ac.za;
mohsensharifpur@duytan.edu.vn

- ¹ Process Design Development Research Group, Center for Process Systems Engineering, Chemical Engineering Department, Universiti Teknologi PETRONAS, 32610 Seri Iskandar Perak, Malaysia
- ² Department of Biosystems Engineering, Tarbiat Modares University, Tehran, Iran
- ³ Thermal Department, School of Mechanical Engineering, National Technical University of Athens, Athens, Greece
- ⁴ Department of Mechanical and Aeronautical Engineering, University of Pretoria, Pretoria 0002, South Africa
- ⁵ Institute of Research and Development, Duy Tan University, Da Nang 550000, Vietnam
- ⁶ Faculty of Bio Engineering and Technology, Advanced Material Cluster, Universiti Malaysia Kelantan, Jeli, Kelantan, Malaysia

c_p Specific heat capacity, J kg⁻¹K⁻¹
 d Receiver tube diameter, m
 f_r Friction factor
 F View factor
 h Convection coefficient, W m⁻²K⁻¹
 h' Internal heat transfer coefficient, Wm⁻²K⁻¹
 k Heat transfer coefficient
 m_2 Slope of linear equation
 \dot{m} Mass flow rate, kg s⁻¹
 Nu Nusselt number
 Pr Prandtl number
 \dot{Q}_{net} Net heat transfer rate, W
 \dot{Q}^* Rate of available solar heat at the receiver cavity, W
 \dot{Q}_{loss} Loss rate of heat from cavity receiver, W
 R Thermal resistance, K/W
 Re Reynolds number
 T Temperature, K
 T_∞ Ambient temperature, K
 t Time, s

PV-HDH desalination modeling

A, a Area, m²
 b Breadth, m

a_{humid}	Surface area of humidifier packing per unit volume, $\text{m}^2 \text{m}^{-3}$
C_f	Conversion factor of the thermal power plant
c_p	Specific heat capacity, $\text{J kg}^{-1} \text{K}^{-1}$
D	Diameter, m
F	Area ratio
F'	Flat plate collector efficiency
F_R	Flow rate factor
G	Dry air mass flow rate, kg s^{-1}
h	Heat transfer coefficient, $\text{W m}^{-2}\text{K}^{-1}$
h_{fg}	Latent heat enthalpy of water vaporization, J kg^{-1}
h_{p1}	Penalty factor due to tedlar through glass, solar cell and EVA
h_{p2}	Penalty factor due to the interface between tedlar and the working fluid
h_T	Heat transfer coefficient from back surface to air through tedlar, $\text{W m}^{-2}\text{K}^{-1}$
H	Enthalpy, kJ kg^{-1}
$I(t)$	Incident solar irradiation, W m^{-2}
K	Thermal conductivity, $\text{W m}^{-1}\text{K}^{-1}$
K_{humid}	Heat transfer coefficient, $\text{kg m}^{-2} \text{s}^{-1}$
\dot{L}	Length, m
L	Sea water flow rate, kg s^{-1}
m	Mass flow rate, kg s^{-1}
m_{fw}	Freshwater production
Nu	Nusselt number, –
Pr	Prandtl number,–
Q_u	Rate of useful energy transfer
Re	Reynolds number,–
T	Temperature, K
T_a	Ambient temperature, K
U	Global heat transfer coefficient, $\text{W m}^{-2}\text{K}^{-1}$
U_b	An overall heat transfer coefficient from water to ambient, $\text{W m}^{-2} \text{K}^{-1}$
U_L	Overall heat transfer coefficient from solar cell to ambient through the back insulation, $\text{W/m}^2 \text{K}$
U_t	Overall heat transfer coefficient from solar cell to ambient through glass cover, $\text{W m}^{-2}\text{K}^{-1}$
U_T	Conductive heat transfer coefficient from solar cell to water through tedlar, $\text{W m}^{-2}\text{K}^{-1}$
U_{tT}	Overall heat transfer coefficient from glass to tedlar through solar cell, $\text{W m}^{-2}\text{K}^{-1}$
U_{tw}	Overall heat transfer coefficient from glass to water through solar cell and tedlar, $\text{W m}^{-2}\text{K}^{-1}$
W	Tube spacing, m
V	Volume, m^3

Greek symbols

α	Absorptivity
β	Packing factor
ε	Emissivity

η	Efficiency
τ	Transmittance
σ	Stefan–Boltzmann constant, $\text{W m}^{-2}\text{K}^{-4}$
ω	Specific humidity

Subscripts

0	Glass to ambient
a	Air
amb	Ambient
Ave	Average
bs	Back surface of tedlar
cond	Due to conduction, Condenser
conv	Due to convection
c	Solar cell
eff	Effective
f	Fluid
f_{out}	Outgoing fluid
fw	Fresh water
G	Glass
humd	Humidifier
in	Inlet
inlet, in	At the inlet
ins, i	Insulation
loss	Energetic loss
n	Tube section number
net	Net
outer, out	Outlet
rad	Due to radiation
rec	Receiver
r	Reference
s	Inner tube surface
T	Tedlar
th	Thermal
total	Total
unit	Unit of desalination
w	Water
zero	Initial condition in the inlet
∞	Ambient

Abbreviations

GOR	Gain output ratio
HDD	Humidification–dehumidification desalination
PV	Photovoltaic
PVT	Photovoltaic-thermal

Introduction

Nowadays, desalination technology is introduced as an interesting research subject due to the scare of freshwater for humans [1]. Moreover, the use of renewable energy sources for desalination is introduced as an interesting subject. There are different kinds of renewable energy, such as solar energy, hydropower, wind energy, and fossil fuel [2–4]. Solar energy

can be employed as the source of thermal energy of the desalination systems [5]. Different kinds of solar collectors can be applied for collecting solar energy including dish concentrator, parabolic trough concentrator (PTC), compound parabolic concentrator (CPC), etc. [6, 7]. The PTC collectors are accounted for as a mature and efficient technology for absorbing solar energy [8]. On the other side, the needed electrical energy for the desalination can be prepared by photovoltaic panels or by organic Rankine cycle (ORC) systems [9, 10]. Different heat sources can be coupled with the ORC system for power generation including waste heat, solar energy, geothermal energy, etc. [11, 12]. Organic fluids, with low boiling point temperatures, are utilized as the ORC fluid for power generation [13]. The ORC heat supply can come from multiple sources such as solar heating, waste heat, and geothermal energy [14]. The main characteristic of the ORC system is that it can generate power from low-temperature heat sources.

There are some researches related to the performance of the PTCs on the basis of numerical and experimental analyses [15–17]. Agagna et al. [18] numerically and experimentally investigated a PTC system performance using the MicroSol-R tests platform. Three numerical models including simple, less complex, and complex models were developed for the estimation performance of the examined system. Three developed models showed an acceptable prediction of the PTC system compared to the results of experimental tests. Song et al. [19] considered an optical model for calculation heat flux using a fast method. They found the calculation time using the suggested method has reduced compared to a three-dimensional model. Houcine et al. [20] suggested a method for calculating the optical performance of a solar PTC system using the ray tracing method. The solar system with different tracking errors, rim angles, and concentration ratios was evaluated. A review by Kumaresan et al. [21] has shown different methods for increasing the performance of a PTC system such as application of the nanofluid, selective coating, and cavity receivers. Srivastava and Reddy [22] designed and investigated a PTC system utilizing alumina/water nanofluid. The performance of the investigated solar PTC system was evaluated with photovoltaic technology. Hoseinzadeh et al. [23] numerically optimized different dimensions of a PTC system in order to achieve the highest performance, through the Monte Carlo method. The optical efficiency of the system increased with increasing the angle of the rim and decreasing the width of the PTC aperture. The modeling was developed using code written in the MATLAB software.

Some researchers have investigated solar desalination systems for producing freshwater [24–35]. Al-Othman et al. [36] simulated a desalination system for the production of desalinated water with 1880 m³ per day. The results showed that the required power was around 63 MW. They found that

two PTC collectors with a combined total aperture area of 3160 m² can supply approximately 76% of the 63 MW power requirements for the desalination system. Elashmawy [6] integrated a tubular solar distiller with a parabolic solar concentrator in Hail, Saudi Arabia. They found a daily efficiency of 36.5%, 30.5% for two investigated experimental setups. In another work [37], a desalination system that had a PTC collector, evacuated tube collector and heat pipe was developed. They found the efficiency of 65.2% for the investigated solar desalination system. Rahbar et al. [38] investigated asymmetrical solar still that was integrated with thermoelectric units for freshwater production. They found the distillate output improved by the suggested system. Palenzuela et al. [39] investigated a multi-effect distillation (MED) with concentrating solar power (CSP) plants. They found fresh water and power production by the investigated system under certain conditions could be compared with the results of a reverse osmosis (RO) system with CSP plants. Mohamed et al. [40] carried out research on a seawater humidification–dehumidification desalination (HDD) technology which was driven by a parabolic trough solar collector in which the outlet temperature does not exceed 100 °C. They found collector thermal efficiency increased with increasing solar irradiance. Also, the desalination system productivity increased when the daytime is getting higher. They reported that the maximum production of the desalination system was calculated equal to 29%, 33%, 37%, and 42% during winter, autumn, spring, and summer, respectively.

Garg et al. [41] designed and theoretically modeled a hybrid HDD module integrated with a nanofluid-based direct absorption solar collector. In this unit, the humidification–dehumidification section and absorber were integrated via a heat exchanger. Graphite nanoparticles were adopted in the solar collector for enhancing the heat transfer process. GOR of the module was estimated for various operational conditions including particle volume fraction, height, and length of the collector, nanofluid mass flow rate within the collector, and incident solar radiation on the collector. Tlili et al. [42] conducted the first and second laws thermodynamics analysis as well as optimization of an HDD system. Exergy analysis showed that the heat source (heater) is the component with the highest exergy destruction. Rafiei et al. [43] numerically investigated the performance of a solar desalination system with a dish concentrator as the heat source. Different shapes of cavity receivers were used as an absorber of the dish concentrator including cylindrical, cubical, and hemispherical cavity receivers. The influence of different shapes of cavity receivers and different operational parameters of the desalination system such as water-to-air flow ratio and the water flow rate was investigated. A humidification–dehumidification desalination technology was used as the desalination system. They found the hemispherical cavity receiver resulted in the highest performance

of the desalination system equal to 19 kg h^{-1} . Lately, Rafiei et al. [44] combined the PV system with the humidification–dehumidification desalination (HDD) systems. The authors presented a novel hybrid solar desalination system, implementing a numerical model. In particular, they focused on nanofluids as solar operating fluid, investigating different oil-based nanofluids. They found that Cu/oil nanofluid exhibits the highest amount of freshwater and the lowest gain output ratio of the desalination system. Lawal et al. [45] proposed a vapor compression heat pump-driven humidification–dehumidification process with energy recovery process. Two systems with different applications of recovered energy were suggested. The cost of freshwater for system without recovery of brine energy reduced by about 15.23% with energy recovered in the system. The gain output ratio, recovery ratio, and productivity of the system were improved by 23%. The proposed modifications to the energy recovery system increased both thermal and economic efficiency of the systems. These results stimulated the need for a rejected recovery of brine energy from the humidification and dehumidification system.

On the other side, the solar desalination system with ORC systems was studied by some researchers as an interesting subject for research [46–48]. Some researchers have modeled power generation systems with different heat sources [49–51]. In the work of Delgado-Torres and García-Rodríguez [52], a solar RO desalination system was applied for the production of freshwater using ORC technology for power generation. They presented some recommendations for designing a more efficient system for producing fresh water and power. Shalaby [53] reviewed the application of ORC and photovoltaic (PV) technology as the source of energy of a solar reverse osmosis desalination system. They studied the influence of different kinds of collectors on the desalination system performance. They recommended the application of the PTC-ORC-RO system as an efficient system for freshwater production. Torres and Rodríguez [54] investigated a solar RO desalination system using the ORC system. The influence of four organic fluids was considered as the working fluids in the ORC. Two configurations of the ORC system including direct and indirect absorption solar energy by the organic fluids were considered. Igobo and Davies [25] experimentally investigated a reverse osmosis desalination system using an ORC system. R245fa was used as the ORC fluid. The industrial bakery facility waste heat was applied as the heat source for the ORC system. They found producing 0.4 L of fresh water per 1 kg of baked food. Ariyanfar et al. [55] developed a humidification–dehumidification desalination system using an ORC system. They assumed outlet water of the ORC system was entered in the desalination system for freshwater production. They found n-heptane as the ORC fluid had resulted the highest freshwater production.

The aforementioned literature review reveals that solar desalination systems with ORC are attractive choices in the energy sector. Regarding this fact, the current work investigates a novel system that incorporates both photovoltaic panels and PTC. Two different kinds of PTC are examined and compared; the conventional PTC with smooth absorber and the PTC with corrugated absorber, which is able to enhance the rates of heat transfer. Moreover, the present ORC system is fed both by the solar field and the hot brine of the humidification–dehumidification desalination (HDD) system. The role of the thermal PV panels is to preheat the saline water and also to generate electricity. Furthermore, the effect of different solar PTC parameters such as the solar irradiation and the oil inlet temperature was evaluated. Also, various parameters of PV-HDD were considered, such as water and air volume flow rate.

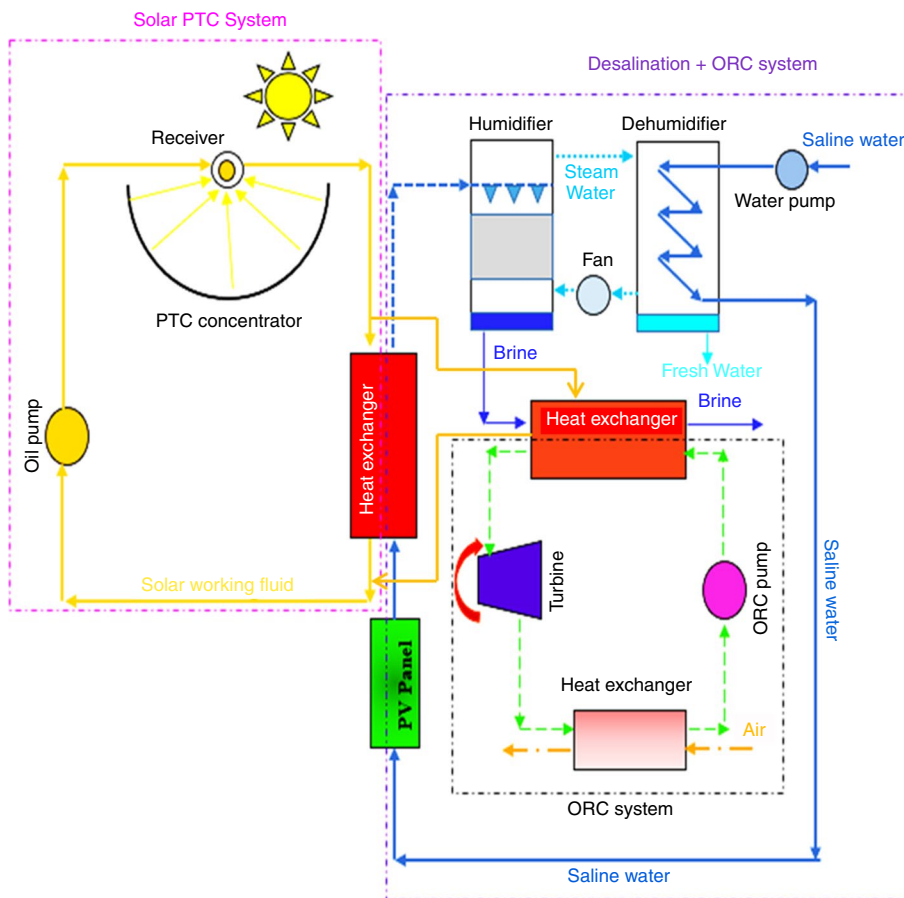
Methodology and modeling

In the present study, a hybrid solar humidification–dehumidification desalination (HDD) system is investigated for producing freshwater and generating power. The solar desalination system consisted of an HDD technology, parabolic trough concentrator (PTC), ORC system and PV panel. A schematic of the hybrid solar desalination system is provided in Fig. 1. The solar PTC system was considered as the thermal source of the desalination unit. The PTC system was evaluated using two kinds of receiver tube, corrugated and smooth types. The ORC technology was used for power generation, and it is fed by the solar field and from the hot brine. The PV panels were used for preheating and generating electricity.

Generally, simulation of the current research is summarized as follows:

- The investigated solar PTC systems were optically and thermally simulated as the desalination heat source using SolTrace and Maple software, respectively. Thermal modeling was conducted on the basis of the energy balance equations.
- Receiver heat gain and surface temperature of the different elements of the PTC receiver were estimated using the obtained internal heat transfer and energy balance equations.
- The heat gain calculated for each type of receiver tubes (of both smooth and corrugated tubes) was applied as the desalination heat source in the next stage.
- The saline water after preheating in the thermal PV panels absorbs the collected solar energy by the PTC system. The heated saline water was entered into the HDD system for desalination. The simulation of the HDD system was

Fig. 1 Schematic of the investigated hybrid system



conducted on the basis of energy and mass equation balances.

- Solar energy is used for feeding the ORC and also the hot brine is used for supplying a part of the heat (as preheating the organic fluid) in the ORC heat exchanger (heat recovery system).
- Investigation of environmental impacts of the suggested solar HDD system for producing fresh water and power.

Flowchart of the determination process is presented in Fig. 2. Simulation and investigation of the solar desalination system are presented in the following sections in detail.

Humidifier–dehumidifier desalination

A schematic of the HDD system is provided in Fig. 3. This system consisted of a water pump for circulating saline water (1 in Fig. 3), PV panels for preheating (2 in Fig. 3), heat exchanger for absorbing energy (3 in Fig. 3), humidifier for spraying and producing saturated vapor from the heated saline water (4 in Fig. 3), a fan for circulating humidify air between the humidifier and dehumidifier units (5 in Fig. 3), and dehumidifier for producing freshwater by cooling the saturated vapor (6 in Fig. 3). The saline

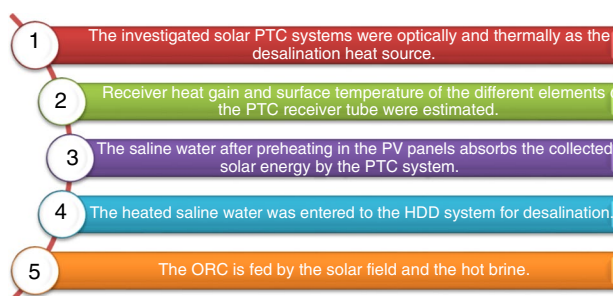


Fig. 2 Flowchart of the calculation process

water was circulated by the water pump in the desalination unit. The saline water after crossing the dehumidifier tubes for cooling the saturated vapor was crossed from the PV panels for preheating. The preheated saline water was entered into the heat exchanger for absorbing energy that was collected by the solar system. Afterward, the heated saline water was sprayed in the humidifier to producing saturated vapor. Then, the saturated vapor was circulated by the fan for passing to the dehumidifier shell. Then fresh water was produced by cooling the humidified air in the dehumidifier unit.

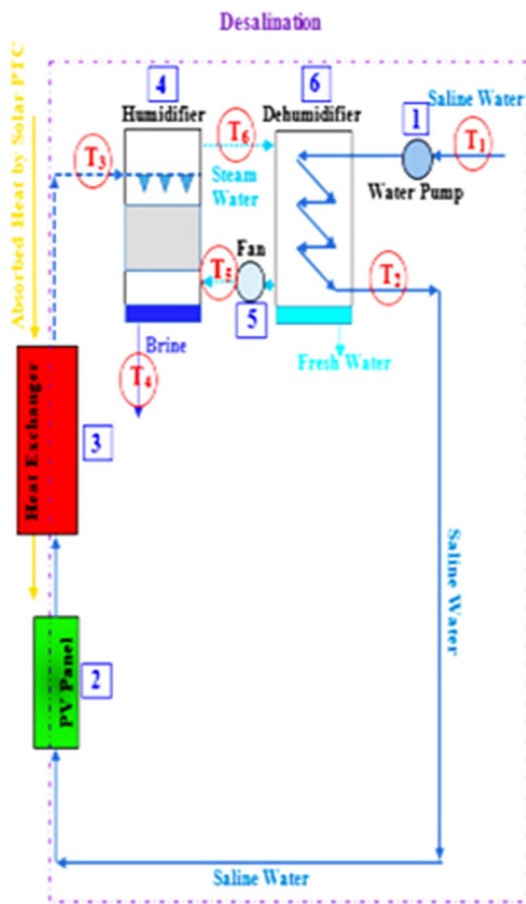


Fig. 3 Schematic of the HDD system

The energy balance equations in the humidifier and dehumidifier systems can be defined based on the following [56]:

$$L C_{p_w} (T_2 - T_1) + 0.5 U_{\text{loss}} A_{\text{unit}} \left(\frac{T_5 + T_6}{2} + T_{\text{amb}} \right) = G (H_6 - H_5) \quad (1)$$

$$L C_{p_w} (T_2 - T_1) = U_{\text{cond}} A_{\text{cond}} \left(\frac{(T_6 - T_2) - (T_5 - T_1)}{\ln \frac{T_6 - T_2}{T_5 - T_1}} \right) \quad (2)$$

$$L C_{p_w} (T_3 - T_4) + 0.5 U_{\text{loss}} A_{\text{unit}} \left(\frac{T_5 + T_6}{2} + T_{\text{amb}} \right) = G (H_6 - H_5) \quad (3)$$

In these equations, L (kg s^{-1}) is saline water mass volume flow rate, C_{p_w} ($\text{kJ kg}^{-1} \text{K}^{-1}$) is water heat capacity, U_{loss} ($\text{W m}^{-2} \text{K}^{-1}$) is heat losses, A_{unit} (m^2) is the area, T_n (K) is fluid temperature, T_{amb} (K) is ambient temperature, G (kg s^{-1}) is dry air mass volume flow rate, H (kJ kg^{-1}) is enthalpy, and U_{cond} ($\text{W m}^{-2} \text{K}^{-1}$) is heat losses. It should be mentioned that subscription numbers are shown in Fig. 3. The mass transfer coefficient in the humidifier unit (K) can

be calculated based on Eq. (3). The average amount of the mass transfer coefficient can be calculated as follows:

$$G (H_6 - H_5) = K a V \left[\frac{(H_3 - H_6) - (H_4 - H_5)}{\ln \frac{H_3 - H_6}{H_4 - H_5}} \right] \quad (4)$$

In this equation, V (m^3) shows the volume of the humidifier, a (m^2) is the surface per unit volume of the humidification column, and H (kJ kg^{-1}) is the enthalpy.

Water heat transfer coefficient in the condenser can be determined based on the Dittus-Boelter relationship as following:

$$\text{Nu} = 0.023 \cdot \text{Re}^{0.8} \cdot \text{Pr}^{0.4} \quad (5)$$

Also, the airside heat transfer coefficient can be estimated as follows [56]:

$$h_a = \frac{0.29 \cdot k_a}{d} \cdot \text{Re}_a^{0.633} \cdot \text{Pr}_a^{\frac{1}{3}} \cdot F^{-0.17} \quad (6)$$

In Eq. (6), F refers to the area ratio between airside and waterside; d denotes the heat exchanger external diameter in the dehumidifier unit. In this research, the mass transfer coefficient was assumed $0.021 \text{ kg m}^{-2} \text{s}^{-1}$, humidifier packing surface area was assumed 300 m^2 , the mass volume flow rate of the saline water was assumed in the range of $1.5\text{--}6.5 \text{ kg s}^{-1}$ [57].

Freshwater production can be defined as the humidity ratio (ω) of the inlet and outlet of humidifier. The freshwater production (m_{fw}) of the desalination system can be determined as follows [58]:

$$m_{\text{fw}} = G \cdot (\omega_2 - \omega_1) \quad (7)$$

Gain output ratio (GOR) can be defined as follows [58]:

$$\text{GOR} = \frac{m_{\text{fw}} h_{\text{fg}}}{Q_u} \quad (8)$$

where Q_u (W) is the absorbed heat by the desalination system.

Solar parabolic trough concentrator

A solar PTC system was considered as the thermal energy source of the desalination unit and of the ORC. The schematic of this system is presented in Fig. 4. The solar PTC system consisted of a parabolic trough concentrator (1 in Fig. 4), an evacuated tube receiver (2 in Fig. 4), a heat exchanger (3 in Fig. 4), and an oil pump (4 in Fig. 4). Behran thermal oil was applied as HTF of the solar system. In the utilized heat exchanger, absorbed solar irradiation by the HTF was transferred to the saline water.

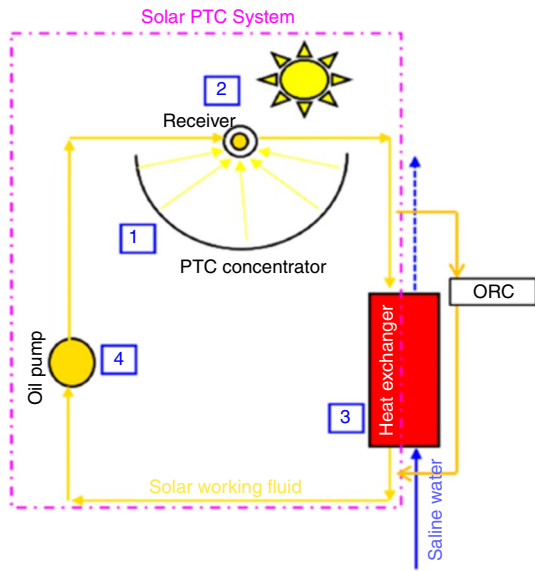


Fig. 4 Schematic of the solar PTC system

The considered solar PTC module had a length and aperture wide of 2 m and 70 cm, respectively. The focal distance and rim angle of the PTC system were assumed to be 17.5 cm and 90°, respectively. The evacuated tube receiver consisted of a receiver tube and a glass cover. The glass cover was utilized for decreasing thermal losses. The diameters of the cover and the receiver were assumed equal to 60 mm and 28 mm, respectively. Two kinds of the receiver tube (corrugated and smooth) were considered as heat sources of the desalination system. The optical analyses of the solar system were conducted in the SolTrace software. The simulated solar PTC system in this software is displayed in Fig. 5. The total solar field is created by using many identical PTC modules connected.

The thermal modeling of the solar system was conducted in the Maple software. The energy balance equation, applied for PTC system modeling, is on the basis of Eq. (9) as:

$$\dot{Q}_{net} = \dot{Q}^* - \dot{Q}_{loss, total} \tag{9}$$

where $\dot{Q}^*(W)$ is the amount of the receiver solar heat flux and $\dot{Q}_{loss, total} (W)$ is cavity receiver total thermal loss. The thermal resistance approach was employed for estimating the amount of cavity receiver heat loss. A view of the cavity receiver and its heat losses is depicted in Fig. 6. The total heat lost from the PTC receiver can be determined on the basis of the below equations. It should be mentioned that a summary of different heat losses is reported in Table 1.

$$\dot{Q}_{loss, total} = \frac{T_s - T_{air}}{R_{total}} \tag{10}$$

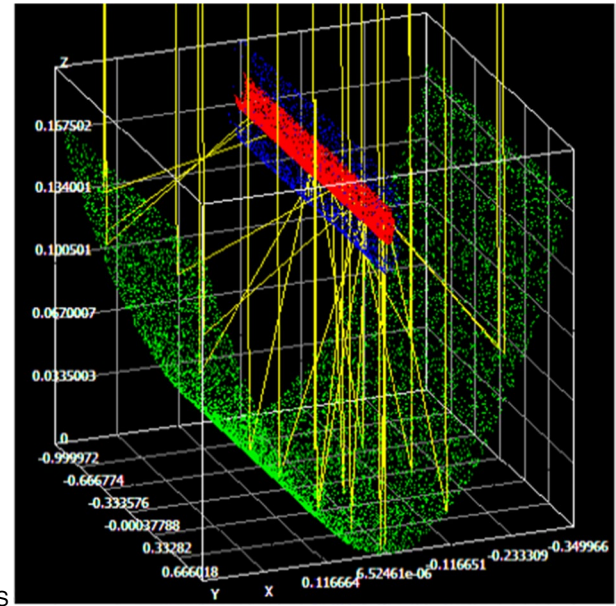


Fig. 5 Simulated solar PTC system in the SolTrace software

$$R_{total} = R_{total,1} + R_{total} + R_{total,2} \tag{11}$$

$$R_{total,1} = \frac{R_1 \times R_2}{R_1 + R_2} \tag{12}$$

$$R_{total,2} = \frac{R_4 \times R_5}{R_4 + R_5} \tag{13}$$

Finally, for estimating the absorbed heat gain, an advanced method was developed based on the deviation of the receiver in smaller elements. The energy balance equation for each element can be calculated as follows:

$$\dot{Q}_{net,n} = \dot{Q}_n^* - \frac{A_n}{R_{total,n}} \cdot (T_{s,n} - T_{\infty}) \tag{14}$$

where $\dot{Q}_n^*(W)$ is the absorbed thermal energy by each element, $A_n (m^2)$ is the element surface area, $R_{total,n}$ is the thermal resistance of each element, $T_{s,n}$ is element surface temperature, and T_{∞} is the ambient temperature.

The internal convection can be calculated as follows:

$$\dot{Q}_{net,n} = \frac{\left(T_{s,n} - \sum_{i=1}^{n-1} \left(\frac{\dot{Q}_{net,i}}{\dot{m} \cdot c_{p0}} \right) - T_{inlet,0} \right)}{\left(\frac{1}{h_{inner} \cdot A_n} + \frac{1}{2 \cdot \dot{m} \cdot c_{p0}} \right)} \tag{15}$$

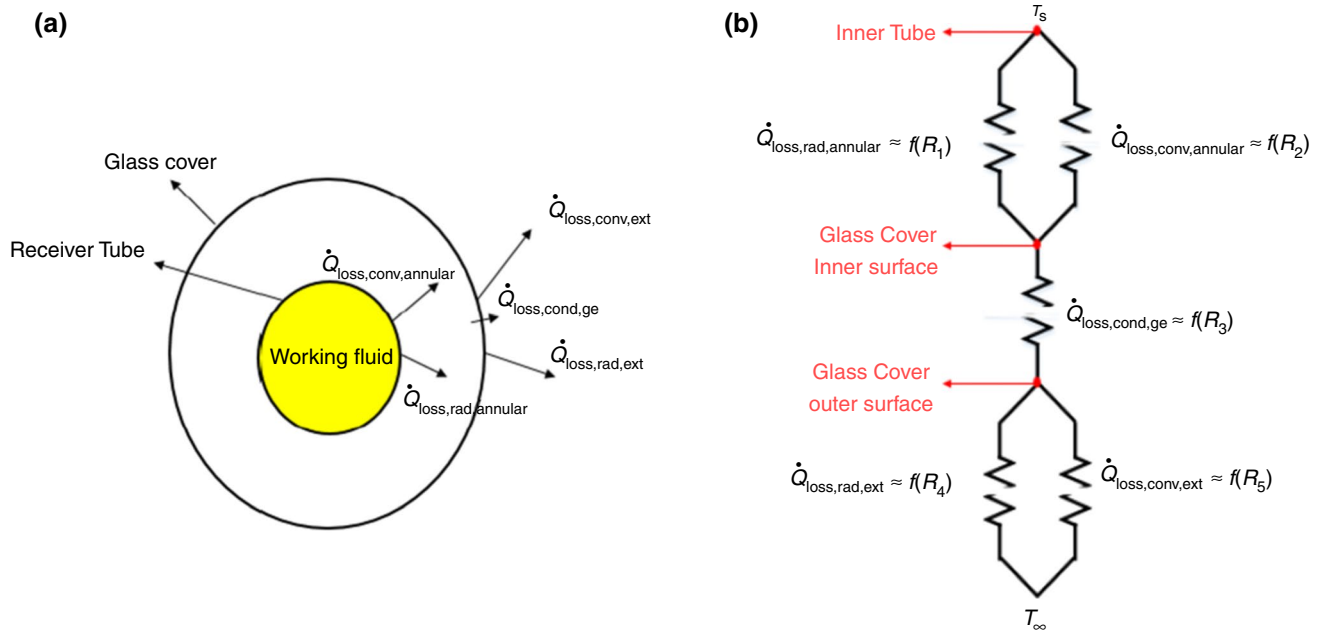


Fig. 6 Schematic of a solar PTC heat losses and b the thermal resistance method [59]

Table 1 A summary of different PTC heat losses

Radiation in annual region/R ₁	$\hat{q}_2 = \frac{\sigma \pi D (T_D^4 - T_d^4)}{\frac{1}{\epsilon_d} + \frac{D(1+\epsilon_D)}{d\epsilon_D}}$
Natural annular convection/R ₂	$h_1 = \frac{1}{\left(\frac{D}{2}\right) \ln\left(\frac{d}{D}\right) + \left(\frac{9\gamma-5}{2(\gamma+1)}\right) \left(2.331 \times 10^{-20} \frac{T_{23}^{23+237}}{P_a \delta^2}\right) \left(\frac{d}{D} + 1\right)}$
Conduction from glass cover/R ₃	$\hat{q}_3 = 2\pi k_{45} \frac{\Delta T_{45}}{\ln \frac{D_5}{D_4}}$
External radiation/R ₄	$q_5 = \sigma \epsilon \pi D (T_D^4 - T_{ci}^4)$
Natural external convection/R ₅	$Nu_{4,natural} = \left[0.6 + \frac{0.378 Ra^{1/6}}{\left(1 + \left(\frac{0.599}{Pr}\right)^{9/16}\right)^{1/4}} \right]^2$
Cross-flow external forced convection/R ₅	$Nu_{4,forced} = c Re^m Pr^n \left(\frac{Pr}{Pr_w}\right)^{1/4}$

$$Nu_{inner} = \frac{\left(\frac{f_r}{8}\right) \cdot Re \cdot Pr}{1 + 12.8 \cdot \sqrt{\frac{f_r}{8}} \cdot (Pr^{0.68} - 1)} \tag{16}$$

where f_r is the friction factor that can be calculated as follows for the smooth and corrugated tubes based on Eqs. (17) and (18), respectively:

$$f_r = 0.316 \cdot Re^{-0.25} + 0.41 \cdot \left(\frac{D_{ri,min}}{D_{ri}}\right)^{0.9} \tag{17}$$

$$f_r = (0.79 \ln Re - 1.64)^{-2} \tag{18}$$

The coefficient of heat transfer is calculated as:

$$h'_{inner} = \frac{Nu_{inner} K_{fluid}}{d_{tube}} \tag{19}$$

The thermal conductivity of the fluid (K_{fluid}) and the inner tube diameter (d_{tube}) are used in the previous equation. Finally, the surface temperature of each element ($T_{s,n}$) and the net rate of heat transfer of each element ($\dot{Q}_{net,n}$) were determined by solving Eqs. (14) and (15) utilizing the Newton–Raphson method [60].

Photovoltaic panel

In the current research, thermal photovoltaic panels were used for preheating the saline water and for power generation. A schematic of the PV panels in the desalination

$$T_{w_out} = \left[\frac{h_{p1}h_{p2}(\alpha\tau)_{eff}I(t)}{U_L} + T_a \right] \left[1 - \exp\left(-\frac{F'A_cU_L}{mC_p}\right) \right] + T_{w_in} \exp\left(-\frac{F'A_cU_L}{mC_p}\right) \tag{23}$$

system is displayed in Fig. 7. According to Fig. 7a, the PV panels were located before the heat exchanger in the desalination system. The saline water was flowed at the PV module backside for enhancing the thermal performance of the PV panels and preheating (as seen in Fig. 7b).

The PV panels consisted of a glass plate for recovery of thermal energy from the module, a PV panel for electricity generation, and a gap for flowing water at the backside of the PV panels. Temperatures of the glass plate (T_{bs}), PV modules (T_c), and the heated water at the outlet gap of PV (T_{w_out}) were presented in Eqs. (20), (21) and (22), respectively. The blackened absorber plate temperature, which is located below the PV module, is determined as [61]:

$$T_{bs} = \frac{h_{p1}(\alpha\tau)_{eff}I(t) + U_{iT}T_a + h_T T_w}{U_{iT} + h_T} \tag{20}$$

The PV cell temperature can be estimated as follows [61]:

$$T_c = \frac{\tau_G[\alpha_c\beta_c + \alpha_T(1 - \beta_c)]I(t) - \eta_c I(t)\beta_c + U_t T_a + U_T T_{bs}}{U_t + U_T} \tag{21}$$

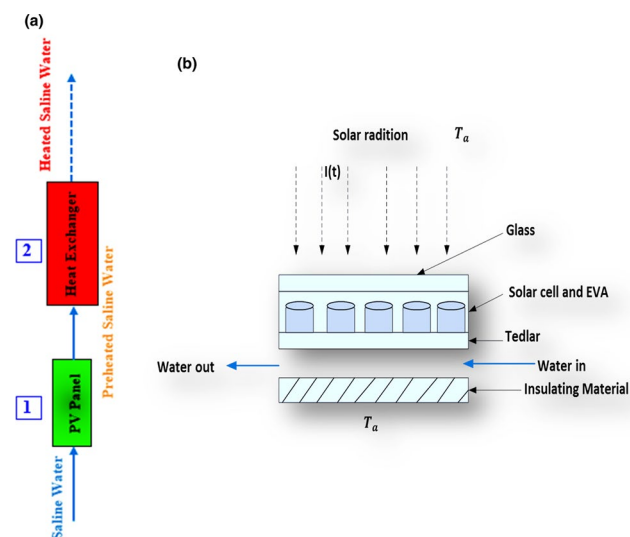


Fig. 7 Schematic of a the PV panels in the desalination system, b cross section of the PV panels

The PV module electrical efficiency can be obtained as:

$$\eta_c = \eta_0 [1 - 0.0045(T_c - 25)] \tag{22}$$

The HTF temperature through the pipe of absorber which located below the PV model can be determined as [61]:

where (T_{w_out}) shows the water outlet temperature, whereby it becomes the inlet temperature for the humidifier column. The available thermal energy rate at the end of the PV module is obtained as follows:

$$Q_u = mC_p(T_{w_out} - T_{w_in}) \tag{24}$$

After substituting the expression for calculating the (T_{w_out}), absorbed heat can be calculated as follows:

$$Q_u = A_c F_R \{ h_{p1}h_{p2}(\alpha\tau)_{eff}I(t) - U_L(T_{w_in} - T_a) \} \tag{25}$$

Organic Rankine cycle system

Organic Rankine cycle was investigated for electricity generation. This device is fed with heat from the solar field and the brine. The solar field gives the main heat input in the ORC, and the brine assists it, especially for preheating the organic fluid in the heat exchanger inlet. More specifically, the brine preheats the organic fluid up to a temperature level, and then the extra heat for the preheating, evaporation and superheating is given by the solar field. So, there is a proper combination of these heat sources in order to utilize the hot brine. A schematic of the ORC system is presented in Fig. 8. The ORC system consists of four components including a pump for ORC fluid circulating in the ORC cycle (1 in Fig. 8), a heat exchanger for transferring the ejected heat by the desalination system to the ORC fluid (2 in Fig. 8), a turbine for generating power (3 in Fig. 8) and a condenser for ejected heat from the ORC system (4 in Fig. 8).

The mass flow of the organic fluid rate was varied based on the absorbed heat in the heat exchanger (or heat recovery system). Consequently, the amount of the mass volume flow rate can be estimated as [62]:

$$\dot{m}_{RC} = \frac{\dot{Q}_{input}}{(h_3^* - h_2^*)} \tag{26}$$

In this equation, \dot{Q}_{input} (W) is absorbed heat in the evaporator, h_3^* (kJ kg^{-1}) and h_2^* (kJ kg^{-1}) are enthalpy of the ORC fluid at the outlet and inlet of the evaporator.

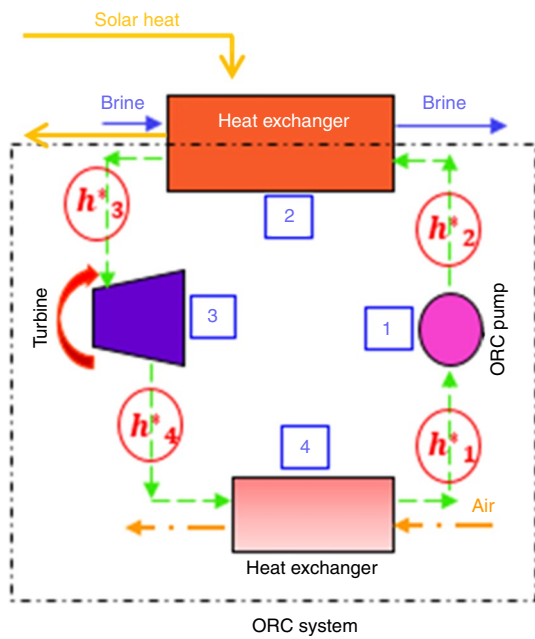


Fig. 8 A schematic of the ORC system

General equations for estimating ORC performance can be calculated as follows [62]:

$$\dot{W}_T = \dot{m}_{RC}(h_3^* - h_4^*) \quad (27)$$

$$\dot{Q}_c = \dot{m}_{RC}(h_4^* - h_1^*) \quad (28)$$

$$\dot{W}_P = \dot{m}_{RC}(h_2^* - h_1^*) \quad (29)$$

$$\dot{W}_{net} = \dot{W}_T - \dot{W}_P = \dot{m}_{RC}[(h_3^* - h_4^*) - (h_2^* - h_1^*)] \quad (30)$$

Finally, the Rankine cycle efficiency and overall efficiency of the solar Rankine cycle can be calculated using Eqs. (31) and (32), respectively.

$$\eta_{RC} = \frac{\dot{W}_{net}}{\dot{Q}_{input}} \quad (31)$$

$$\eta_{overall} = \frac{\dot{W}_{net}}{I_{beam} \cdot A_{ap,PTC}} \quad (32)$$

It should be mentioned that seven organic fluids were selected including R245ca, R134a, R113, R152a, R245fa, R11, and R141b. All of the ORC fluids were studied close to the optimum turbine inlet temperature as reported by Ref. [59].

Environmental aspects

The utilization of renewable-energy-based systems is highly recommended owing to their positive impacts on decreasing the emission of greenhouse gases. In the current paper, the environmental effects of the application of solar energy as the desalination thermal energy source, and ORC technology for power production from the waste thermal energy of the desalination system were investigated. The annual amounts of mitigated CO₂ can be determined as [63]:

$$\varphi_{CO_2} = \frac{\psi_{CO_2} \times E_{en,ann}}{10^3} \quad (33)$$

where φ_{CO_2} (ton) refers to the annual emission of CO₂, ψ_{CO_2} (kgCO₂ kWh⁻¹) denotes mean production of CO₂ for generating power by using coal that was considered equal to 2.04, and $E_{en,ann}$ (kWh) is annual generated power by employing ORC or solar. In this study, Tehran in Iran is considered as the case study and 2500 h is assumed for a year. Moreover, the carbon credit (Z_{CO_2}) was considered in this study in addition to the previous parameters as follows [63]:

$$Z_{CO_2} = z_{CO_2} \times \varphi_{CO_2} \quad (34)$$

where Z_{CO_2} (\$) is annual carbon credit, z_{CO_2} (\$) per ton refers to carbon credit that is considered equal to 14.5, and φ_{CO_2} (ton) is the annual emission of CO₂ [63].

Validation of the developed model

Humidifier–dehumidifier desalination modeling

The numerical modeling of the HDD unit was validated using the reported result by Franchini and Perdichizzi [64]. A solar HDD system with the reported dimensions in Table 2 was considered by them. Figure 9 shows a comparison of the production of fresh water versus seawater temperature data obtained in the current research, against the reported results by Franchini and Perdichizzi [64]. It was seen that an acceptable agreement was found between the results in this study when compared to the data from them. Practically, the literature points and the found points by the developed model are identical, and so the validation procedure proves the validity of the developed model.

Tables 3 and 4 show the fluid properties achieved by the HDD unit and the design and performance parameters of the HDD unit.

Table 2 The condenser and humidifier parameters [64]

	Heat exchange Surface/m ²	Width/m	Depth/m	Height/m
Condenser	1500	1.0	1.0	3.75
Humidifier	300	1.0	1.0	1.5

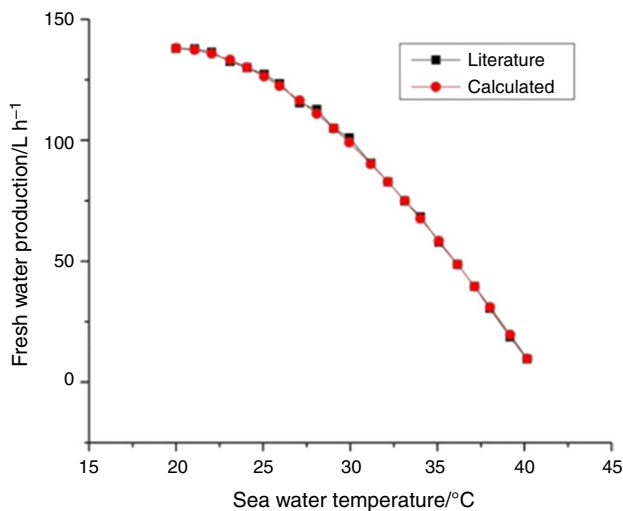


Fig. 9 Comparison of current results and reported resulted by Ref. [64]

Solar system

The thermal modeling of the solar system was validated with reported experimental results by Kasaeian et al. [65]. The experimental setup structural dimensions are similar to the dimensions of the applied system in the present work (see Table 5). Consequently, the results of the current research can be validated with the measured data by Kasaeian et al.

Table 3 Fluid properties for HDD unit

Fluids properties					
Water			Air		
Point	Properties		Points	Properties	
1	$T/^\circ\text{C}$	27.5	5	$T/^\circ\text{C}$	39.3
	$H/\text{kJ kg}^{-1}$	115		$H/\text{kJ kg}^{-1}$	160
2	$T/^\circ\text{C}$	35.6	6	Specific Humid (kg per kg dry air)	0.0469
	$H/\text{kJ kg}^{-1}$	148.8		Relative Humidity	100%
3	$T/^\circ\text{C}$	53	6	$T/^\circ\text{C}$	45.1
	$H/\text{kJ kg}^{-1}$	221.5		$H/\text{kJ kg}^{-1}$	214
4	$T/^\circ\text{C}$	45	6	Specific Humid (kg per kg dry air)	0.0655
	$H (\text{kJ kg}^{-1})$	188.1		Relative Humidity	100%
Fresh Water	$T/^\circ\text{C}$	39.3			
	$H/\text{kJ kg}^{-1}$	164.3			

Table 4 Design and performance parameters of the HDD unit

Design parameters	
Sea water flow rate $L/\text{kg s}^{-1}$	0.28
L/G ratio	1.5
Performance parameters	
Fan power/kW	0.045
Fresh water production/ kg hr^{-1}	12.47
Fresh water on seawater percentage/%	1.2

Table 5 Dimensions of steel mirror reflector [65]

Parameter	Value
Length/ L_c	2 m
Width/ w	70 cm
Focal length/ f	17.5 cm
Aperture/ A_a	1.4 m ²
Rim angle/ φ	90°
Mean thickness	0.8 mm

[65]. Experimental setup schematic by them is displayed in Fig. 10. Figure 11 illustrates a comparison between the present numerical data and the ones reported by them. As seen in Fig. 11, the numerical results obtained in this study have shown good agreement with the measured experimental data by Kasaeian et al. [65] with the mean deviation to be around 3%. This deviation is a reasonable value and acceptable because it is lower than the uncertainty of the experimental results of Ref. [65], which was about 3.6%. So, the found results are inside the experiential error limits and it can be said that the developed model is reliable. Moreover, it is obvious that higher operating temperature leads to lower efficiency both in the results of this work and of the literature, and so these curves have similar trends.

Fig. 10 A schematic of the experimental setup in Ref. [65]

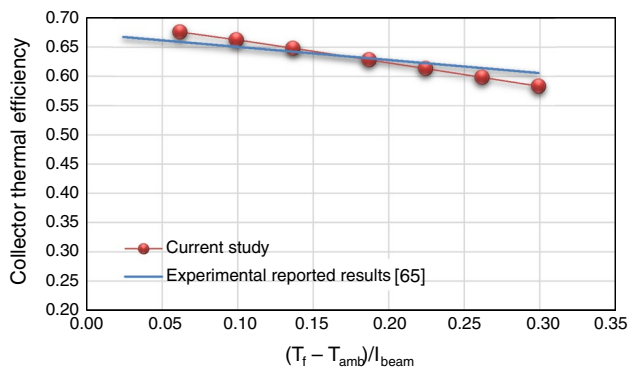
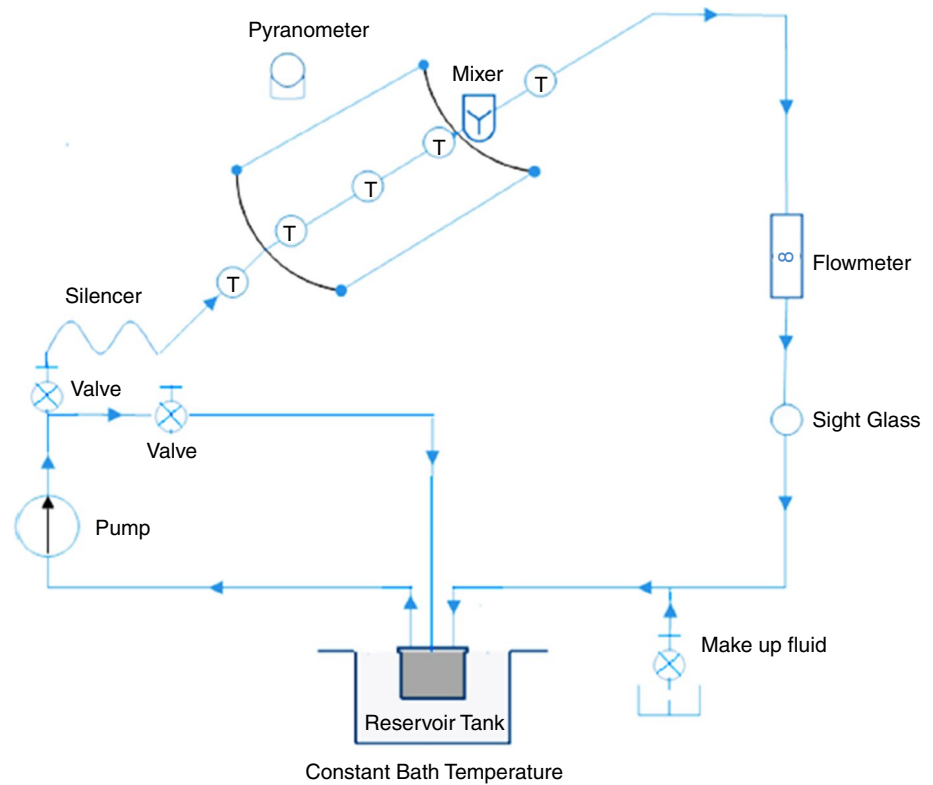


Fig. 11 Comparison of the results of the current study against the reported results from [65]

Results and discussion

In the first part of this section, the solar and desalination system performance was reported. Also, the performance of the coupled ORC system was presented. Finally, the environmental impacts of the suggested solar desalination system were presented in detail.

Energy and fresh water productivity analyses

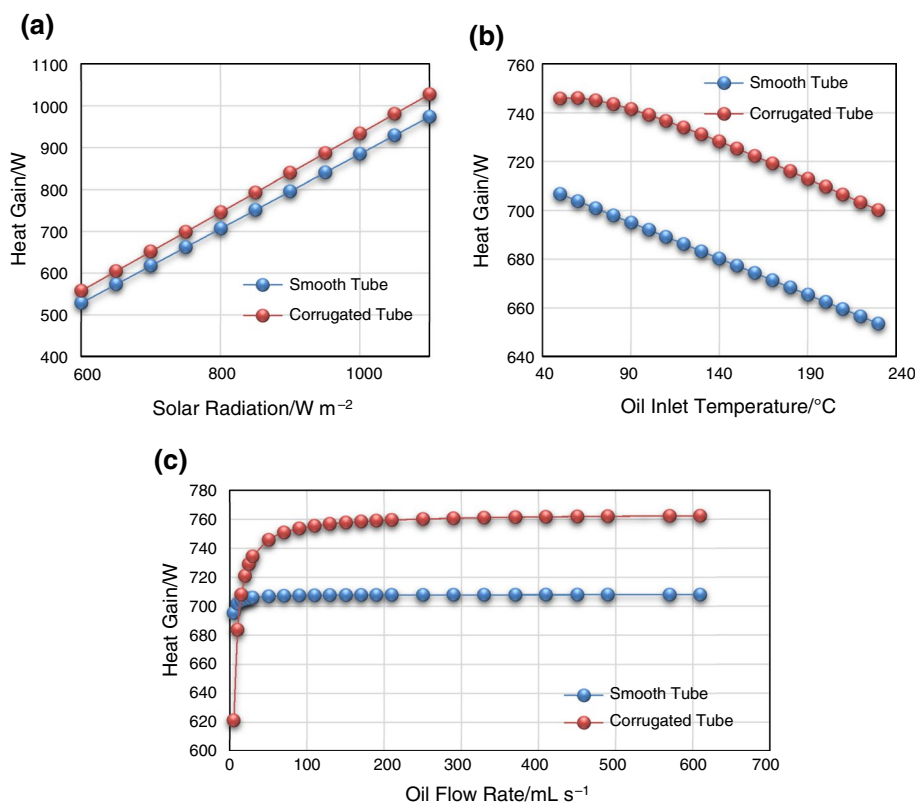
This section presents the performance of solar energy and the desalination system based on the change of condition and

operational parameters including solar irradiance, oil inlet temperature, oil volume flow rate, water volume flow rate, water inlet temperature, etc.

Energy performance

Figure 12a–c shows the change of heat gain of the solar PTC system under changes in solar irradiance, oil inlet temperature, and oil volume flow rate for corrugated and smooth tubes as the evacuated tube receiver, respectively. It would be seen in Fig. 12a that as solar irradiance increases, heat gain increases linearly for the two investigated tubes. The corrugated tube values are greater than the corresponding values in the smooth one. The minimum values of heat gain for smooth and corrugated tubes are 528.63 W and 557.79 W for solar irradiance of 600 W m^{-2} , respectively, and maximum heat gain values for those are 974.02 W and 1027.83 W for solar irradiance of 1100 W m^{-2} at oil volume flow rate of 50 mL s^{-1} , and constant oil inlet temperature on $50 \text{ }^\circ\text{C}$, respectively. On the other side, it could result from Fig. 12b that as oil inlet temperature increases, heat gain decreases. It seems the relation between oil inlet temperature and heat gain to be almost linear for the smooth tube, but certainly nonlinear for corrugated tube specifically in lower oil inlet temperature values. In this region, the relation for corrugated tube has less slope before point number 4 ($90 \text{ }^\circ\text{C}$, 741.45 W) than after it, and then it becomes linear. Finally, as seen

Fig. 12 Change of heat gain with changing **a** solar irradiance, **b** oil inlet temperature and **c** oil volume flow rate (for the PTC module)

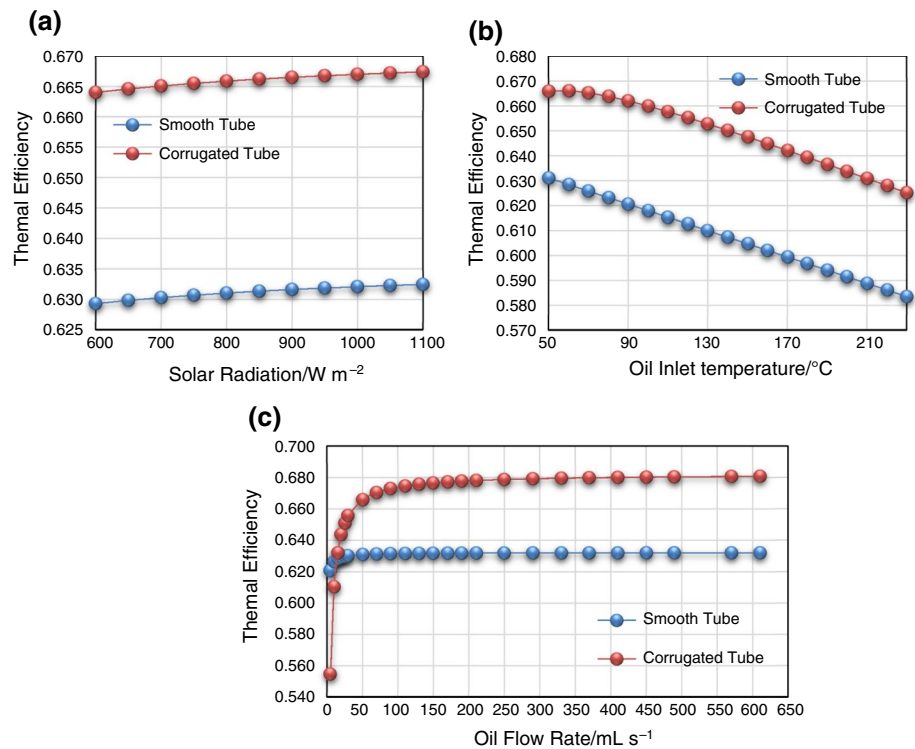


in Fig. 12c, heat gain by the PTC system has increased with increasing solar HTF volume flow rate for both kinds of the receiver tube, including the corrugated and smooth tubes. Also, the corrugated tube resulted in higher heat gain with increasing oil volume flow rate compared to the smooth one. The minimum values of heat gain for smooth and corrugated tubes are 695.26 W and 621.25 W for oil volume flow rate of 5 mL s⁻¹, respectively, and maximum heat gain values for those are 707.97 W and 762.50 W for oil volume flow rate of 60 mL s⁻¹ at constant solar irradiance of 800 W m⁻², and constant oil inlet temperature on 50 °C, respectively. The heat gain of the PTC system increased until 15 mL s⁻¹ and 170 mL s⁻¹ for the smooth and corrugated tube, and then the increase in heat remained almost constant, respectively. Consequently, increasing the oil volume flow rate upper than 15 mL s⁻¹ and 170 mL s⁻¹ for the smooth and corrugated tubes is not recommended, respectively, because higher oil volume flow rate generally had caused increasing pressure drop and pumping power-consuming compared to increasing the solar PTC system thermal performance (see “Appendix A”). It could be concluded from the above-mentioned results that for achieving a higher amount of heat gain, a lower inlet temperature of the solar working fluid, the optimum amount of flow rate of the working fluid, and higher solar radiation, are suggested.

For the above conditions, the thermal efficiency changes under changing solar irradiance, oil inlet

temperature, and oil volume flow rate are shown in Fig. 13a–c, respectively. As seen in Fig. 13a, with the increase in solar irradiance, the thermal efficiency of the solar system is enhanced for both kinds of the receiver tube. Also, the corrugated tube resulted in higher thermal efficiency than the smooth one. The solar PTC system thermal efficiency has ranged from 0.629 to 0.632 for the smooth tube, and from 0.664 to 0.667 for the corrugated one. The highest amount of the thermal efficiency was equal to 66.74% for the corrugated tube with solar irradiance of 1100 W m⁻², oil volume flow rate of 50 mL s⁻¹, and oil inlet temperature of 50 °C. As shown in Fig. 13b, with increasing oil inlet temperature, the thermal efficiency of the solar PTC system with both smooth and corrugated tubes decreased. Also, the corrugated tube resulted in higher thermal efficiency than the smooth one. Thermal efficiency had changed between 62.22–66.59% and 62.41–63.11% for the corrugated tube and the smooth tube was based on the constant solar irradiance of 800 W m⁻², and constant oil volume flow rate of 50 mL s⁻¹, respectively. The highest system thermal efficiency was obtained as 66.59% for oil temperature of 50 °C, solar irradiance of 800 W m⁻², and oil volume flow rate of 50 mL s⁻¹. Finally, the change of thermal efficiency was reported for the oil volume flow rate in the bound of 5 mL s⁻¹ to 610 mL s⁻¹. The solar irradiance was assumed to be equal to 800 W m⁻², and oil inlet

Fig. 13 Change of thermal efficiency with the changing of **a** solar irradiance, **b** oil inlet temperature, and **c** oil volume flow rate



temperature was assumed to be equal to $50^{\circ}C$ in Fig. 13c. As understood from Fig. 13c, the solar PTC system thermal efficiency had shown enhancing with increasing oil volume flow rate for both investigated receiver tubes. Also, the corrugated tube resulted in higher thermal efficiency in comparison with the smooth tube as the solar PTC receiver. The thermal efficiency of the PTC system was varied between 55.47 and 68.08% for the corrugated tube, and between 62.08 and 63.21% for the smooth one. Also, optimum values of oil volume flow rate of $15 mL s^{-1}$ and $170 mL s^{-1}$ for the smooth and corrugated tube can be recommended based on the presented discussion in the previous section. Similar to the presented conclusion in the previous paragraph, for achieving a higher thermal performance of the solar system, the use of lower inlet temperature of the solar working fluid, the optimum amount of flow rate of the working fluid, and higher solar radiation is recommended. Also, the application of the corrugated receiver tube is suggested for higher thermal performance.

Freshwater production

The change of fresh water production versus the change of solar irradiance and oil volume flow rate is presented in Fig. 14. Two types of tube including corrugated and smooth tubes were assessed as the PTC receiver. The water volume flow rate and water-to-air ratio of the desalination system were assumed equal to $0.28 kg s^{-1}$ and 1.5,

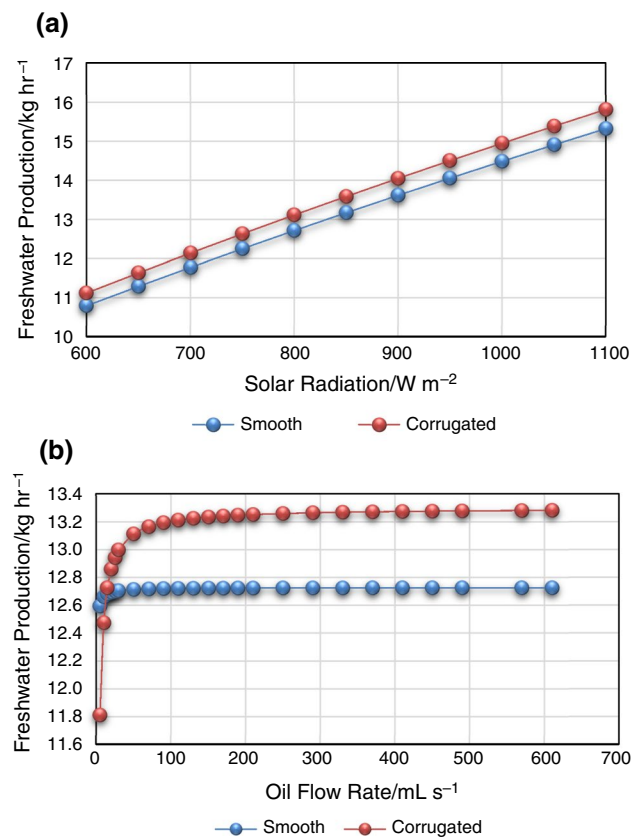


Fig. 14 Change of freshwater production with the change of **a** solar irradiance and **b** oil volume flow rate with smooth and corrugated tubes at $L/G=1.5$ and $L=0.28 m$

respectively. As seen in Fig. 14a, the output relations are linear, and the produced freshwater for the corrugated tube is more than that of for smooth one. In other words, the freshwater production increases with the solar irradiance increase for both types of receiver tubes. The reason for this is in a higher amount of PTC heat gain with increasing solar irradiance, as discussed in the previous section. Freshwater production varied from 11.12 to 15.82 kg hr⁻¹ for the corrugated tube and changed from 10.80 to 15.32 kg hr⁻¹ for the smooth one. Also, Fig. 14b presents based on the change of the oil volume flow rate between 5 mL s⁻¹ to 610 and a constant solar irradiance of 800 W m⁻². As resulted from Fig. 14b, higher amounts of the freshwater were calculated with the application of higher amounts of oil volume flow rate for both investigated tubes. This is because of increasing heat gain with increasing oil volume flow rate as discussed in the previous section. Also, the corrugated tube had resulted in higher freshwater production compared to the smooth one. The average freshwater productions were estimated equal to 13.09 kg hr⁻¹ and 12.71 kg hr⁻¹ for the corrugated and smooth tubes, respectively. Also, optimum values of oil volume flow rate of 15 mL s⁻¹ and 170 mL s⁻¹ for the smooth and corrugated tube can be recommended based on the presented discussion in the previous section. It could have resulted that for achieving a higher amount of freshwater, the lower inlet temperature of the solar working fluid, the optimum amount of flow rate of the working fluid, and higher solar radiation are suggested. Also, the application of the corrugated receiver tube is more effective for producing a higher amount of freshwater.

Freshwater production versus the change of solar irradiance at different amounts of water volume flow rate and

different values of water-to-air flow ratio (LG) for smooth tube is presented in Fig. 15a, b, respectively. As shown in Fig. 15a, the impact of different amounts of the water volume flow rate was investigated on freshwater production of the desalination system at constant water-to-air ratio of 1.5. As seen in Fig. 15a, higher amounts of the water volume flow rate and solar irradiance resulted in higher freshwater production. On the other side, as shown in Fig. 15b influence of different amounts of water-to-air ratio was studied on freshwater production of the desalination system at a constant water volume flow rate of 0.28 kg s⁻¹. As resulted from Fig. 15b, with increasing water-to-air ratio in the desalination system, freshwater production decreases. Consequently, a higher amount of water flow and a lower value of the water-to-air ratio can be recommended for achieving a higher amount of freshwater production. On the other hand, the influence of inlet water temperature on freshwater production is presented in Fig. 16 for different amounts of water volume flow rate. Also, the water-to-air ratio was assumed to be equal to 1.5. As seen in Fig. 16, increasing water inlet temperature resulted in decreasing freshwater production.

Gain output ratio (GOR)

Figure 17 shows the change of the gain output ratio versus the solar irradiance change and the oil volume flow rate change. The evacuated tube receiver of the PTC system was investigated with smooth and corrugated tubes. As understood from Fig. 17a, the gain output ratio decreased with the increase in solar irradiance for both types of receiver tubes. Moreover, Fig. 17b depicts the change of the oil volume flow rate from 5 to 610 mL s⁻¹ and a constant solar

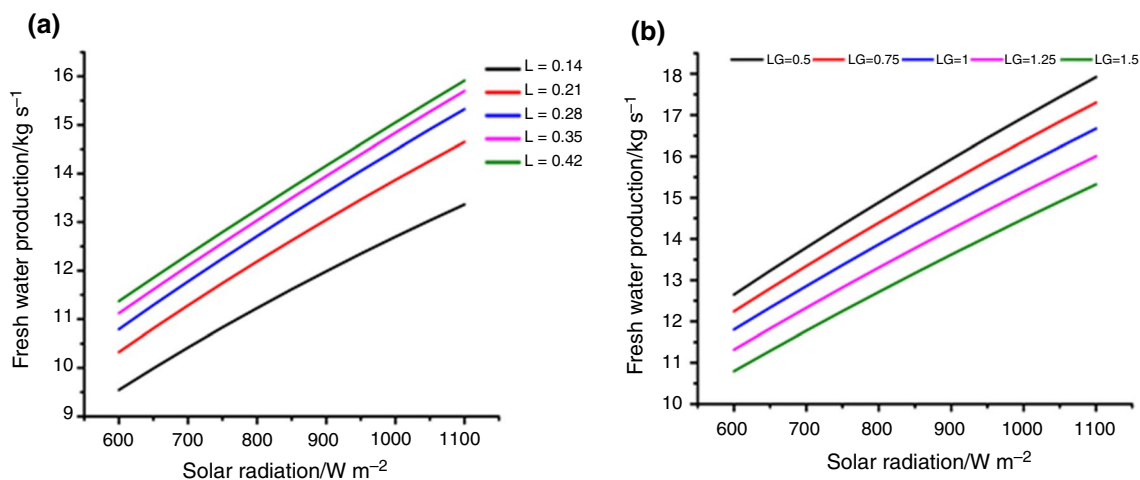


Fig. 15 Freshwater production versus the change of solar irradiance at **a** different inlet water volume flow rate (L), and **b** water-air flow ratio (LG) for smooth tube

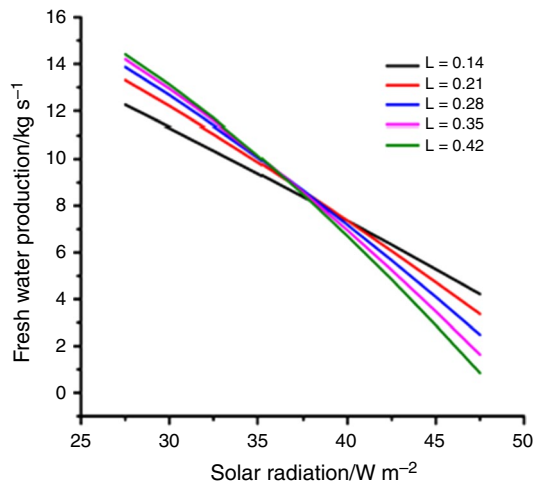


Fig. 16 Freshwater production versus change water inlet temperatures at different inlet water volume flow rate (L)

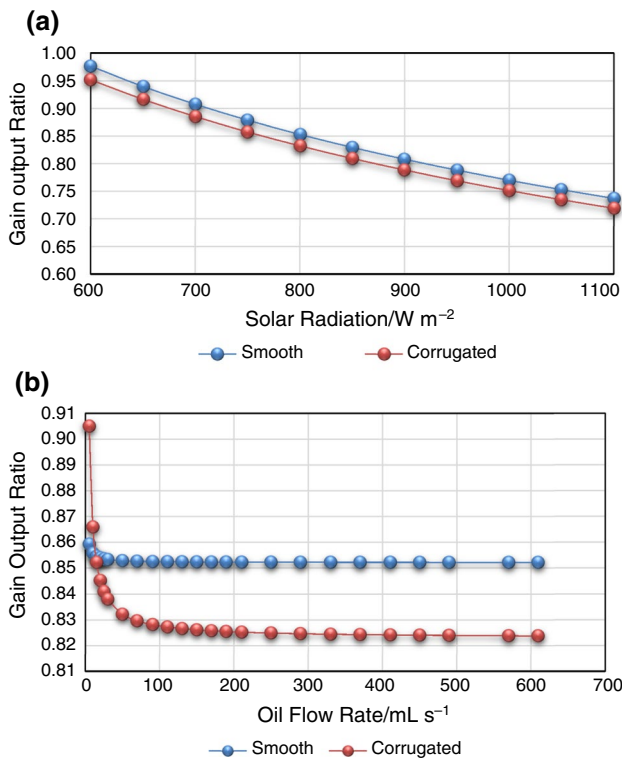


Fig. 17 Change of gain output ratio with the change of **a** solar irradiance and **b** oil volume flow rate with smooth and corrugated tubes at $L/G = 1.5$ and $L = 0.28$ m

irradiance of 800 W m^{-2} . As concluded from Fig. 17b, higher values of the gain output ratio were calculated with the application of lower amounts of oil volume flow rate for both investigated tubes. Also, the smooth tube had resulted in a higher gain output ratio than the corrugated tube. It

could be concluded that for achieving a lower amount of the gain output ratio, lower inlet temperature of the solar working fluid, the optimum amount of flow rate of the working fluid, and higher solar radiation are suggested. Also, the application of the corrugated receiver tube is more effective for reducing the amount of the gain output ratio.

Figure 18a, b presents change of gain output ratio versus solar irradiance change at different amounts of water volume flow rate and different values of water-to-air flow ratio (LG), respectively. Figure 18a depicts different amounts of the water volume flow rate at constant water-to-air ratio of 1.5. As resulted from Fig. 18a, the gain output ratio improved with increasing solar irradiance and increasing water volume flow rate. On the other side, Fig. 18b is presented for different values of water-to-air ratio at a constant water volume flow rate of 0.28 kg s^{-1} . As understood from Fig. 18b, with increasing water-to-air ratio in the desalination system, the gain output ratio decreases. On the other hand, Fig. 19 shows the variations in the gain output ratio versus change in inlet water temperature. Different values of water volume flow rate were examined with a water-to-air ratio equal to 1.5 times. As observed, with increasing the water inlet temperature, gain output ratio decreases.

ORC and PV generated power

Change of ORC power generation versus a change of solar irradiance and the oil volume flow rate for different organic fluids is presented in Fig. 20a, b, respectively. The evacuated receiver tube with the corrugated tube was investigated as the solar PTC absorber. The desalination system was investigated at a constant water volume flow rate of 0.28 kg s^{-1} , and a water-to-air ratio of 1.5. The influence of different organic fluids was studied including R134a, R245ca, R113, R11, R245fa, R152a, and R141b. The ORC system was investigated at a condenser temperature of $38 \text{ }^\circ\text{C}$, and the ORC fluids were investigated at optimum turbine inlet temperature as reported by Shahverdi et al. [59]. The ORC is fed by heat from the PTC and also the brine is used for preheating the organic fluid. As seen in Fig. 20a, the ORC system had resulted in the highest and lowest performance with the application of R113, and R134a as the ORC fluids, respectively. Also, it could be resulted that with increasing solar irradiance, the ORC net work increases. The ORC net work of the ORC system was varied between 4.09 kW and 7.57 kW for R113 as the ORC fluids and from 2.34 kW to 4.33 kW for R134a as the ORC fluids. Figure 20b shows the change of ORC net work versus a change of oil volume flow rate. As seen in Fig. 20b, the

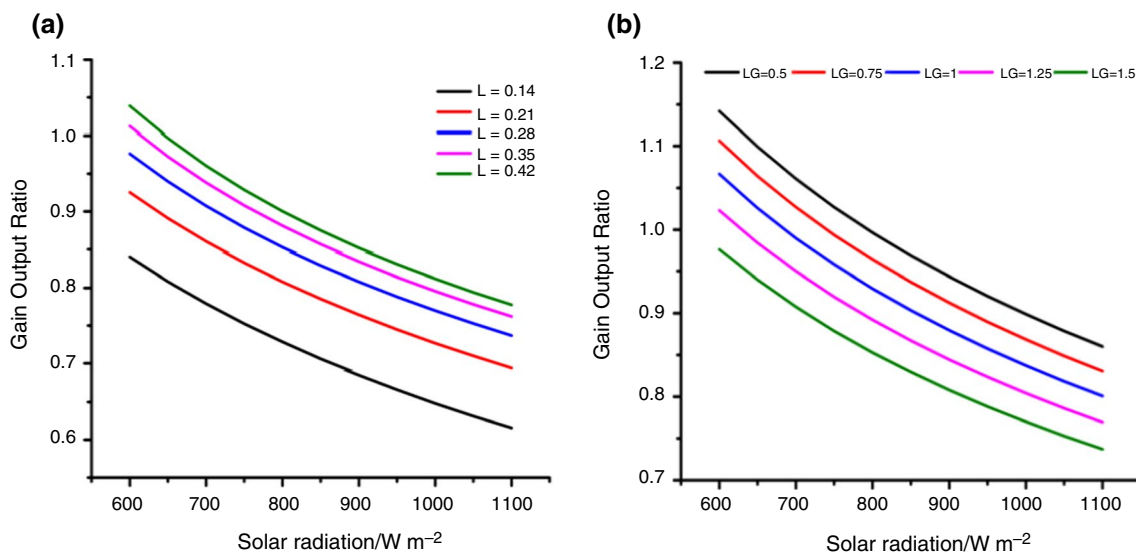


Fig. 18 Gain output ratio versus change of solar irradiance at **a** different inlet water volume flow rate (L) and **b** water-air flow ratio (LG)

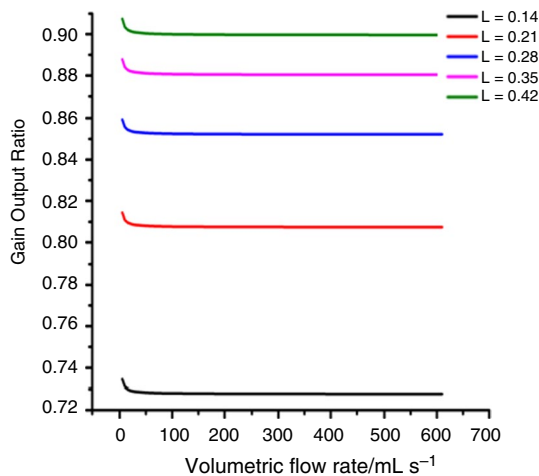


Fig. 19 Gain output ratio versus change water inlet temperatures at different inlet water volume flow rate (L)

ORC net work had enhanced with increasing oil volume flow rate until a limited amount and after that, values of that remained almost constant. Consequently, an optimum value of the oil volume flow rate equal to 170 mL s⁻¹ for the corrugated tube can be recommended. Also, the ORC system had the highest and lowest ORC net work using R113 and R134a, respectively.

Finally, the change of generated power by PV panels versus the change of water inlet temperature at different water volume velocities and water-to-air ratio equal to 1 is presented in Fig. 21. As seen, the generated power by the panels increased

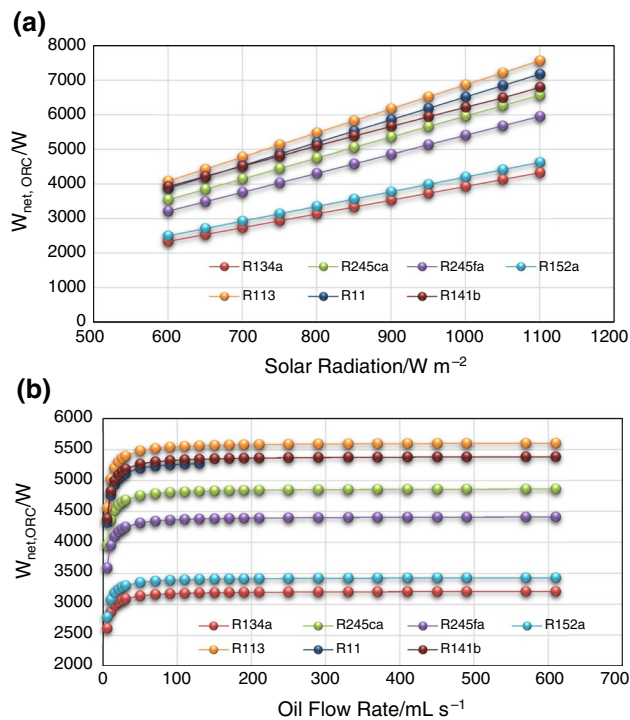


Fig. 20 Change of ORC power generation with the change of **a** solar irradiance and **b** oil volume flow rate for different organic fluids for the corrugated tube at L/G = 1.5 and L = 0.28 kg s⁻¹

with decreasing water inlet temperature and increasing water volume flow rate. The highest amount of generated power was calculated to be nearly 3.29 kW for water inlet temperature of 27.5 °C and water volume flow rate of 0.28 kg s⁻¹.

Fig. 21 Change of generated power by PV panels versus the change of water inlet temperature at different water volume flow rate and water/air ratio of 1

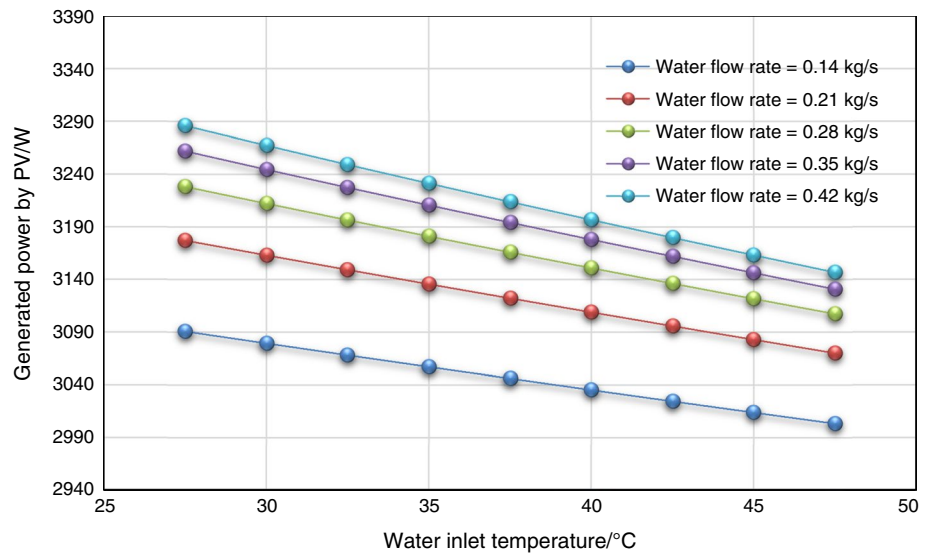


Table 6 Freshwater production, energy generation, and environmental impacts nexus of the suggested solar HDD system with ORC technology

I_{sun} (W m^{-2})	\dot{m}_{FW} (kg h^{-1})	$\dot{W}_{\text{net,ORC}}$ (W)	PTC		ORC	
			φ_{CO_2} (ton CO_2)	Z_{CO_2} (\$)	φ_{CO_2} (ton CO_2)	Z_{CO_2} (\$)
600	11.12	4089.37	85.34	1237.46	54.88	795.81
650	11.63	4437.19	92.53	1341.74	59.55	863.50
700	12.14	4785.04	99.73	1446.02	64.22	931.19
750	12.63	5132.92	106.92	1550.29	68.89	998.89
800	13.11	5480.82	114.11	1654.57	73.56	1066.60
850	13.59	5828.75	121.30	1758.85	78.23	1134.31
900	14.05	6176.72	128.49	1863.13	82.90	1202.02
950	14.50	6524.72	135.68	1967.41	87.57	1269.74
1000	14.95	6872.76	142.88	2071.69	92.24	1337.47
1050	15.39	7220.83	150.07	2175.97	96.91	1405.21
1100	15.81	7568.95	157.26	2280.25	101.58	1472.96

Environmental effects

Table 6 reports the amounts of freshwater production, the ORC power generation, and the environmental impacts of the suggested solar HDD system with ORC technology versus a change of the solar irradiance. It could be seen that the suggested desalination system with the application of the solar system and ORC technology, in addition to producing freshwater in important amounts, significantly reduced amounts of CO₂ emissions in the environment. It should be mentioned that reported CO₂ mitigated (φ_{CO_2}) and carbon credits (Z_{CO_2}) are per annum. Consequently, the application of the suggested solar-ORC desalination system is recommended for freshwater production, power generation, and environmental protection.

Conclusions

In the present article, a solar humidifier–dehumidifier desalination (HDD) system was analyzed. A solar parabolic trough concentrator with smooth and corrugated tubes was applied as the desalination heat source. Moreover, there is an organic Rankine cycle (ORC) system for generating power. Various conditions and operational parameters of the solar PTC, HDD, and ORC systems were investigated. Performance of the solar PTC and the HDD system was studied based on amounts of heat gain, freshwater production, thermal efficiency, gain heat ratio, etc. Also, the environmental effects of the suggested solar desalination system were investigated based on amounts of carbon credits and CO₂ mitigation per annum. The most important outcomes of the current study could be summarized as follows:

- It was concluded that the solar PTC system thermal efficiency varied between 62.22 and 66.59% for the corrugated tube and between 62.41 and 63.11% for the smooth tube at constant solar irradiance of 800 W m^{-2} and constant at an oil volume flow rate of 50 mL s^{-1} .
- The optimum volume flow rate of the solar HTF was recommended to be 15 mL s^{-1} for the smooth and 170 mL s^{-1} for the corrugated tube.
- Freshwater production of the HDD system is enhanced by increasing solar irradiance and by increasing the volume flow rate of the solar HTF. Also, the produced freshwater for the corrugated tube was more than that of for smooth one. The average freshwater productions were estimated at 13.09 kg hr^{-1} and 12.71 kg hr^{-1} for the corrugated and smooth tubes, respectively.
- It was concluded that higher saline water flow and lower value of the saline water-to-air ratio could be recommended for achieving a higher value of freshwater production. Also, the production of freshwater decreased with increasing water inlet temperature.
- The ORC system resulted in the highest and lowest performance with the application of R113 and R134a as the ORC fluids, respectively. Considering the results, solar irradiance increases with increasing ORC net work. The ORC net work of the ORC system was var-

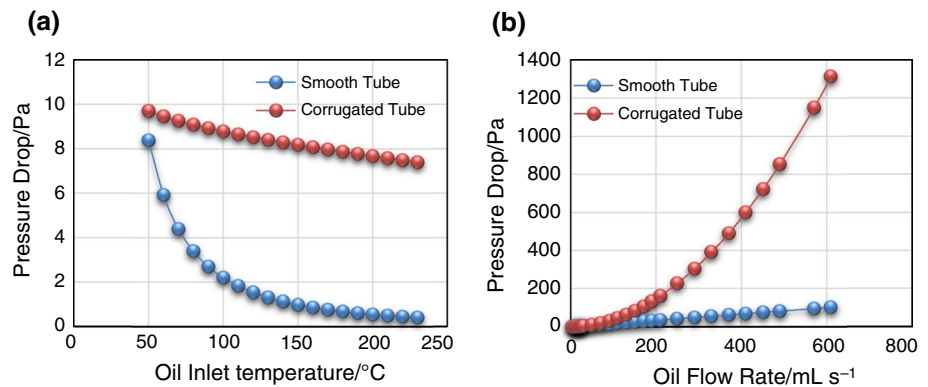
ied between 4.09 kW and 7.57 kW for R113 as the ORC fluid and from 2.34 kW to 4.33 kW for R134a as the ORC fluid.

- It was found that the application of the suggested solar HDD system produces high amounts of freshwater and significantly reduces the equivalent CO_2 emissions to the environment. Considering the results and having positive environmental impacts, the application of the suggested solar-ORC HDD system is recommended for freshwater production and power generation.
- In the future, different topologies of the examined system can be investigated in order to determine the global optimum design. Moreover, different working fluids and especially natural refrigerants can be studied in order to maximize the ORC efficiency.

Appendix A: Pressure drop

Change of pressure drop with changing oil inlet temperature and oil volume flow rate for the smooth and corrugated tube at $I_{\text{beam}} = 800 \text{ W m}^{-2}$ and $VF_{\text{oil}} = 50 \text{ mL s}^{-1}$ is given in Fig. 22.

Fig. 22 Change of pressure drop with changing oil inlet temperature, and oil volume flow rate for the smooth and corrugated tube at $I_{\text{beam}} = 800 \text{ W m}^{-2}$, and $VF_{\text{oil}} = 50 \text{ mL s}^{-1}$



Funding Dr. Najafi and Dr. Loni are grateful to the Tarbiat Modares University (<http://www.modares.ac.ir>) for the financial supports given under IG/39705 grant for Renewable Energies of Modares research group.

References

- Shahzad MW, Burhan M, Son HS, Oh SJ, Ng KC. Desalination processes evaluation at common platform: a universal performance ratio (UPR) method. *Appl Therm Eng.* 2018;134:62–7.
- Khoobakht G, Akram A, Karimi M, Najafi G. Exergy and energy analysis of combustion of blended levels of biodiesel, ethanol and diesel fuel in a DI diesel engine. *Appl Therm Eng.* 2016;99:720–9.
- Hoseini S, Najafi G, Ghobadian B, Mamat R, Ebadi M, Yusaf T. Novel environmentally friendly fuel: the effects of nanographene oxide additives on the performance and emission characteristics of diesel engines fuelled with *Ailanthus altissima* biodiesel. *Renew Energy.* 2018;125:283–94.
- Ghanbari M, Najafi G, Ghobadian B, Yusaf T, Carlucci A, Kiani MKD. Performance and emission characteristics of a CI engine using nano particles additives in biodiesel-diesel blends and modeling with GP approach. *Fuel.* 2017;202:699–716.
- Fouda A, Nada S, Elattar H, Rubaiee S, Al-Zahrani A. Performance analysis of proposed solar HDH water desalination systems for hot and humid climate cities. *Appl Therm Eng.* 2018;144:81–95.
- Elashmawy M. An experimental investigation of a parabolic concentrator solar tracking system integrated with a tubular solar still. *Desalination.* 2017;411:1–8.
- Korres D, Bellos E, Tzivanidis C. Investigation of a nanofluid-based compound parabolic trough solar collector under laminar flow conditions. *Appl Therm Eng.* 2019;149:366–76.
- Chen Q, Yuan Z, Guo Z, Zhao Y. Practical performance of a small PTC solar heating system in winter. *Sol Energy.* 2019;179:119–27.
- Nafey A, Sharaf M. Combined solar organic Rankine cycle with reverse osmosis desalination process: energy, exergy, and cost evaluations. *Renew Energy.* 2010;35:2571–80.
- Mohammed MK, Awad OI, Rahman M, Najafi G, Basrawi F, Abd Alla AN, Mamat R. The optimum performance of the combined cycle power plant: a comprehensive review. *Renew Sustain Energy Rev.* 2017;79:459–74.
- Acar MS, Arslan O. Energy and exergy analysis of solar energy-integrated, geothermal energy-powered Organic Rankine Cycle. *J Therm Anal Calorim.* 2019;137:659–66.
- Arslan O, Ozgur M, Kose R. Electricity generation ability of the Simav geothermal field: a technoeconomic approach. *Energy Sour Part A Recovery Util Environ Eff.* 2012;34:1130–44.
- Liu C, Gao T. Off-design performance analysis of basic ORC, ORC using zeotropic mixtures and composition-adjustable ORC under optimal control strategy. *Energy.* 2019;171:95–108.
- Bellos E, Tzivanidis C. Investigation of a hybrid ORC driven by waste heat and solar energy. *Energy Convers Manag.* 2018;156:427–39.
- Aichouba A, Merzouk M, Valenzuela L, Zarza E, Kasbadji-Merzouk N. Influence of the displacement of solar receiver tubes on the performance of a parabolic-trough collector. *Energy.* 2018;159:472–81.
- Mansour K, Boudries R, Dizene R. Optical, 2D thermal modeling and exergy analysis applied for performance prediction of a solar PTC. *Sol Energy.* 2018;174:1169–84.
- Zhang L, Fan L, Hua M, Zhu Z, Wu Y, Yu Z, Hu Y, Fan J, Cen K. An indoor experimental investigation of the thermal performance of a TPLT-based natural circulation steam generator as applied to PTC systems. *Appl Therm Eng.* 2014;62:330–40.
- Agagna B, Smaili A, Falcoz Q, Behar O. Experimental and numerical study of parabolic trough solar collector of MicroSol-R tests platform. *Exp Thermal Fluid Sci.* 2018;98:251–266.
- Song J, Tong K, Li L, Luo G, Yang L, Zhao J. A tool for fast flux distribution calculation of parabolic trough solar concentrators. *Sol Energy.* 2018;173:291–303.
- Houcine A, Maatallah T, El Alimi S, Nasrallah SB. Optical modeling and investigation of sun tracking parabolic trough solar collector basing on Ray Tracing 3Dimensions-4Rays. *Sustain cities Soc.* 2017;35:786–98.
- Kumaresan G, Sudhakar P, Santosh R, Velraj R. Experimental and numerical studies of thermal performance enhancement in the receiver part of solar parabolic trough collectors. *Renew Sustain Energy Rev.* 2017;77:1363–74.
- Srivastava S, Reddy K. Simulation studies of thermal and electrical performance of solar linear parabolic trough concentrating photovoltaic system. *Sol Energy.* 2017;149:195–213.
- Hoseinzadeh H, Kasaeian A, Shafii MB. Geometric optimization of parabolic trough solar collector based on the local concentration ratio using the Monte Carlo method. *Energy Convers Manag.* 2018;175:278–87.
- Mansouri MT, Amidpour M, Ponce-Ortega JM. Optimal integration of organic Rankine cycle and desalination systems with industrial processes: energy–water–environment nexus. *Appl Therm Eng.* 2019;158:113740.
- Igobo O, Davies P. Isothermal Organic Rankine Cycle (ORC) driving Reverse Osmosis (RO) desalination: experimental investigation and case study using R245fa working fluid. *Appl Therm Eng.* 2018;136:740–6.
- Seyednezhad M, Sheikholeslami M, Ali JA, Shafee A, Nguyen TK. Nanoparticles for water desalination in solar heat exchanger. *J Therm Anal Calorim.* 2020;139:1619–36.
- Omara AA, Abuelnuor AA, Mohammed HA, Khiadani M. Phase change materials (PCMs) for improving solar still productivity: a review. *J Therm Anal Calorim.* 2020;139:1585–617.
- Modi KV, Jani HK, Gamit ID. Impact of orientation and water depth on productivity of single-basin dual-slope solar still with Al_2O_3 and CuO nanoparticles. *J Therm Anal Calorim.* 2020:1–15.
- Ashtiani S, Hormozi F. Design improvement in a stepped solar still based on entropy generation minimization. *J Therm Anal Calorim.* 2020;140:1095–106.
- Suresh C, Shanmugan S. Effect of water flow in a solar still using novel materials. *J Therm Anal Calorim.* 2019:1–14.
- Kabeel A, Sathyamurthy R, El-Agouz S, El-Said EM. Experimental studies on inclined PV panel solar still with cover cooling and PCM. *J Therm Anal Calorim.* 2019;138:3987–95.
- Dhivagar R, Sundararaj S. Thermodynamic and water analysis on augmentation of a solar still with copper tube heat exchanger in coarse aggregate. *J Therm Anal Calorim.* 2019;136:89–99.
- Kumar TS, Jegadheeswaran S, Chandramohan P. Performance investigation on fin type solar still with paraffin wax as energy storage media. *J Therm Anal Calorim.* 2019;136:101–12.
- Sasikumar C, Manokar AM, Vimala M, Winston DP, Kabeel A, Sathyamurthy R, Chamkha AJ. Experimental studies on passive inclined solar panel absorber solar still. *J Therm Anal Calorim.* 2020;139:3649–60.
- Kabeel A, Abdelgaied M, Mahmoud G. Performance evaluation of continuous solar still water desalination system. *J Therm Anal Calorim.* 2020:1–10.
- Al-Othman A, Tawalbeh M, Assad MEH, Alkayyali T, Eisa A. Novel multi-stage flash (MSF) desalination plant driven by parabolic trough collectors and a solar pond: a simulation study in UAE. *Desalination.* 2018;443:237–44.
- Mosleh HJ, Mamouri SJ, Shafii M, Sima AH. A new desalination system using a combination of heat pipe, evacuated

- tube and parabolic trough collector. *Energy Convers Manag.* 2015;99:141–50.
38. Rahbar N, Esfahani JA, Asadi A. An experimental investigation on productivity and performance of a new improved design portable asymmetrical solar still utilizing thermoelectric modules. *Energy Convers Manag.* 2016;118:55–62.
 39. Palenzuela P, Zaragoza G, Alarcón-Padilla D-C. Characterisation of the coupling of multi-effect distillation plants to concentrating solar power plants. *Energy.* 2015;82:986–95.
 40. Mohamed AI, El-Minshawy N. Theoretical investigation of solar humidification–dehumidification desalination system using parabolic trough concentrators. *Energy Convers Manag.* 2011;52:3112–9.
 41. Garg K, Khullar V, Das SK, Tyagi H. Parametric study of the energy efficiency of the HDH desalination unit integrated with nanofluid-based solar collector. *J Therm Anal Calorim.* 2019;135:1465–78.
 42. Tlili I, Osman M, Barhoumi E, Alarifi I, Abo-Khalil AG, Praveen R, Sayed K. Performance enhancement of a humidification–dehumidification desalination system. *J Therm Anal Calorim.* 2020;140:309–319.
 43. Rafiei A, Alsagri AS, Mahadzir S, Loni R, Najafi G, Kasaeian A. Thermal analysis of a hybrid solar desalination system using various shapes of cavity receiver: cubical, cylindrical, and hemispherical. *Energy Convers Manag.* 2019;198:111861.
 44. Rafiei A, Loni R, Mahadzir SB, Najafi G, Pavlovic S, Bellos E. Solar desalination system with a focal point concentrator using different nanofluids. *Appl Therm Eng.* 2020;174:115058.
 45. Lawal DU, Antar MA. Investigation of heat pump-driven humidification–dehumidification desalination system with energy recovery option. *J Therm Anal Calorim.* 2020;1–18.
 46. Abdulkareem MA, Assad MEH, Sayed ET, Soudan B. Recent progress in the use of renewable energy sources to power water desalination plants. *Desalination.* 2018;435:97–113.
 47. Shayesteh AA, Koohshekan O, Ghasemi A, Nemati M, Mokhtari H. Determination of the ORC-RO system optimum parameters based on 4E analysis; Water–Energy–Environment nexus. *Energy Convers Manag.* 2019;183:772–90.
 48. Bruno JC, Lopez-Villada J, Letelier E, Romera S, Coronas A. Modelling and optimisation of solar organic rankine cycle engines for reverse osmosis desalination. *Appl Therm Eng.* 2008;28:2212–26.
 49. Arslan O, Yetik O. ANN modeling of an ORC-binary geothermal power plant: simav case study. *Energy Sources Part A Recovery Util Environ Eff.* 2014;36:418–28.
 50. Arslan O. Power generation from medium temperature geothermal resources: ANN-based optimization of Kalina cycle system-34. *Energy.* 2011;36:2528–34.
 51. Ozgur M, Arslan O, Kose R, Peker K. Statistical evaluation of wind characteristics in Kutahya, Turkey. *Energy Sources Part A.* 2009;31:1450–63.
 52. Delgado-Torres AM, García-Rodríguez L. Design recommendations for solar organic Rankine cycle (ORC)–powered reverse osmosis (RO) desalination. *Renew Sustain Energy Rev.* 2012;16:44–53.
 53. Shalaby S. Reverse osmosis desalination powered by photovoltaic and solar Rankine cycle power systems: a review. *Renew Sustain Energy Rev.* 2017;73:789–97.
 54. Delgado-Torres AM, García-Rodríguez L. Preliminary design of seawater and brackish water reverse osmosis desalination systems driven by low-temperature solar organic Rankine cycles (ORC). *Energy Convers Manag.* 2010;51:2913–20.
 55. Ariyanfar L, Yari M, Aghdam EA. Proposal and performance assessment of novel combined ORC and HDD cogeneration systems. *Appl Therm Eng.* 2016;108:296–311.
 56. Hou S, Ye S, Zhang H. Performance optimization of solar humidification–dehumidification desalination process using Pinch technology. *Desalination.* 2005;183:143–9.
 57. Elsafi AM. Integration of humidification-dehumidification desalination and concentrated photovoltaic-thermal collectors: energy and exergy-costing analysis. *Desalination.* 2017;424:17–26.
 58. Huang B, Lin T, Hung W, Sun F. Performance evaluation of solar photovoltaic/thermal systems. *Sol Energy.* 2001;70:443–8.
 59. Shahverdi K, Loni R, Ghobadian B, Monem M, Gohari S, Marofi S, Najafi G. Energy harvesting using solar ORC system and Archimedes Screw Turbine (AST) combination with different refrigerant working fluids. *Energy Convers Manag.* 2019;187:205–20.
 60. Cengel YA, Ghajar AJ, Kanoglu M. Heat and mass transfer: fundamentals & applications. New York: McGraw-Hill; 2011.
 61. Zubair MI, Al-Sulaiman FA, Antar M, Al-Dini SA, Ibrahim NI. Performance and cost assessment of solar driven humidification dehumidification desalination system. *Energy Convers Manag.* 2017;132:28–39.
 62. Cengel YA. *Thermodynamics An Engineering Approach 5th Edition* By Yunus A Cengel: ThermodynamicsAn Engineering Approach, Digital Designs, 2011.
 63. Sahota L, Tiwari G. Exergoeconomic and enviroeconomic analyses of hybrid double slope solar still loaded with nanofluids. *Energy Convers Manag.* 2017;148:413–30.
 64. Franchini G, Perdichizzi A. Modeling of a solar driven HD (Humidification-Dehumidification) desalination system. *Energy Procedia.* 2014;45:588–97.
 65. Kasaeian A, Daviran S, Azarian RD, Rashidi A. Performance evaluation and nanofluid using capability study of a solar parabolic trough collector. *Energy Convers Manag.* 2015;89:368–75.

Publisher's Note Springer Nature remains neutral with regard to jurisdictional claims in published maps and institutional affiliations.